Feature Extraction and Connectionist Classification of SODAR Echograms

Swati Choudhury and Sushmita Mitra, *Senior Member, IEEE*

Abstract—Sonic detection and ranging (SODAR) systems are efficient and economical tool to probe the lower planetary boundary layer on a continuous basis. The lower atmospheric patterns (each depicting a different atmospheric condition) recorded by this system can prove to be extremely useful if classified and interpreted correctly. The manual identification of these SODAR patterns is a laborious task and requires considerable expertise. A connectionist system has already been developed by the authors to automate the process to some extent. In this letter, we enhance its generalization of performance, by incorporating feature extraction using the fast Fourier transform. The results are compared with that in earlier work to demonstrate its effectiveness.

Index Terms—Acoustic remote sensing, classification, fast Fourier transform (FFT), neural networks, sonic detection and ranging (SODAR) identification.

I. Introduction

SONIC detection and ranging (SODAR) (or acoustic radar) plays a very significant role in probing of the lower planetary boundary layer (LPBL). This is because the interaction of sound waves with the lower atmosphere is stronger as compared to the electromagnetic spectrum. It can be designed at a reasonable cost and is capable of providing the three-dimensional (height, time, and intensity) view of the lower atmospheric microstructures, appearing during different time, month, and season, over a particular region. The observations are termed as SODAR echograms, as the system records the backscattered echoes (sound pulse) [2], [3].

Potential use of SODAR data can be made, provided it can be interpreted and identified correctly. Manual identification of SODAR recorded observations is time-consuming and completely dependent on the knowledge and experience of the experts in this field. Utilization of the full potential of SODAR observations on a global basis calls for the existence of automated techniques, developed preferably by incorporating human expertise.

Artificial neural networks (ANNs) or connectionist models [4] attempt to replicate the *computational* power of biological neural networks and, thereby, endow machines with some of the *cognitive abilities* that biological organizms possess. The Multilayer perceptron (MLP) is a well-known feedforward ANN model that is typically used in pattern classification problems, involving supervised learning in data-rich domains.

Efforts have been made to handle the analysis of voluminous atmospheric data using standard statistical and mathematical methods [5], like Bayes classifier, k-nearest neighbor classifier, etc. MLPs have also been applied to the prediction of tornado and damaging wind conditions [6], [7]. A fuzzy MLP has been employed to successfully classify radio-refraction conditions of the tropospheric environment, categorized as subrefraction, normal-refraction, and superrefraction [8]. It holds promise in tropospheric wireless communication, meteorology, and related fields.

Realizing the utility of SODAR echograms, the Bayes classifier and k-nearest neighbor classifier have been used to distinguish between two classes of SODAR patterns, *viz*, convective thermal plumes and temperature inversion [9]. An elementary attempt to classify the SODAR patterns has been done using fractal feature [10]. Fractal dimension (FD) has been estimated for a few SODAR patterns, and it is shown that FD values change between patterns.

The authors have developed a connectionist approach to successfully classify six different types of echograms recorded by a 2350-Hz monostatic SODAR system [1]. Single-layer structures of the LPBL were categorized as: 1) convective plumes; 2) inversion with flat top; 3) inversion with small spikes; 4) inversion with tall spikes; 5) rising inversion; and 6) rising inversion with convective plumes. These are depicted in Figs. 1–6 part (a) respectively, and modeled as the six input classes of the MLP. The input consisted of random sets of 30 sequential observations from the corresponding echograms.

In this letter, we attempt to extend the connectionist approach [1], by incorporating feature extraction from the SODAR echogram using the fast Fourier transform (FFT) at the input. Thereby, the generalization of classification performance is found to improve. The proposed system is able to jointly exploit the powerful signal processing capability of FFT and parallelism, self-learning and fault tolerance characteristics of ANN models. Its effectiveness is demonstrated by comparing the results obtained from the FFT-based MLP with those obtained using only the standard MLP.

Section II presents a brief description of different types of SODAR echograms being identified, and their corresponding FFT spectrum. Implementation details and comparative results with a related model [1], are provided in Section III. Finally, the letter is concluded in Section IV.

II. SODAR Echograms With FFT

In real life, a function $h(t)$ is sampled at discrete, evenly spaced intervals (Δ) in time. We can estimate its Fourier transform, to obtain its amplitude $H(f)$ in the corresponding frequency domain, from N consecutive sampled points. For $h_k = h(t_k)$, $t_k \equiv k\Delta$, for $k = 0, 1, 2, 3, \ldots, N - 1$, and n
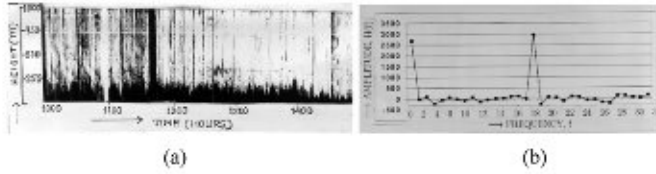
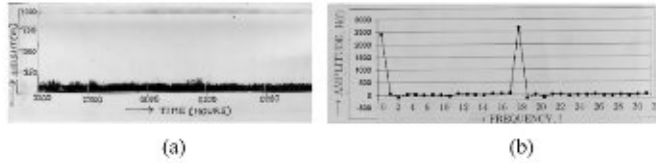Fig. 1.   Convective plumes. (a) Echogram and (b) its FFT.

Fig. 2.   Inversion with flat top. (a) Echogram and (b) its FFT.

$0, 1, 2, 3, \ldots, N - 1$, the discrete Fourier transform H_n is expressed as [11]

$$H_n = \sum_{k=0}^{N-1} h_k e^{-2\pi i k n / N} \tag{1}$$

with the corresponding FFT being [12]

$$\begin{aligned} H_n &= \sum_{k=0}^{N-1} e^{-2\pi i k n / N} h_k \\ &= \sum_{k=0}^{N/2-1} e^{2\pi i n k / (N/2)} h_{2k} + e^{2\pi i n / N} \sum_{k=0}^{N/2-1} e^{2\pi i n k / (N/2)} h_{2k+1}. \end{aligned} \tag{2}$$

A 2350-Hz monostatic SODAR system installed at the Indian Statistical Institute, Kolkata (22°N, 88°E), India, has been used to record the formation of thermal plumes and different types of inversion layers in LPBL. Interested readers may refer to literature [1] for further details. In this letter (as in [1]), we choose to concentrate on the six basic types of single layer structures (each representing a different thermodynamic state of the LPBL) that appeared at our site on more than 80% occasions, during observations recorded over a complete year. The corresponding echograms are depicted in Figs. 1–6, part (a). Part (b) of these figures represent the FFTs of 64 consecutive data samples, chosen from each class.

In all the figures, in part (b) the amplitude of $H(f)$ attained high values at $f = 1$ and $f = 18$. However, it is to be noted that these amplitudes at $f = 1$ and $f = 18$ for classes 1–6 are, respectively, 2700 and 3000; 2400 and 2700; 2800 and 2600; 3000 and 3000; 2500 and 2000; and 1400 and 1900.

Fig. 1(a) depicts the formation of a typical convective boundary layer, representing an unstable atmospheric condition, and is seen to appear on cloudless, clear sunny days of all the four different seasons prevalent over the Indian subcontinent. Transfer of heat, momentum, and energy occurs between the surface and the higher levels, thereby introducing in-mixing within the layers.

Fig. 2(a) describes the formation of ground-based temperature inversion layer in the LPBL, approximately 150 m thick
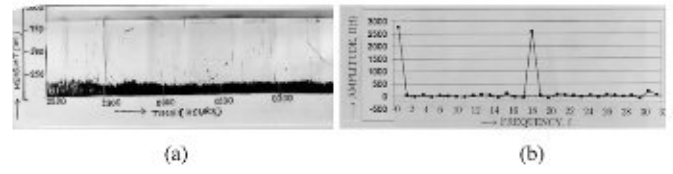

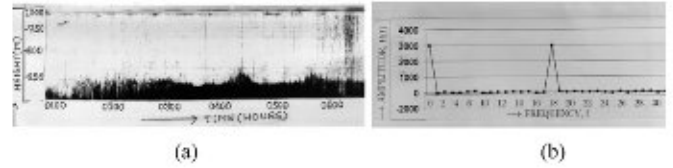Fig. 3.   Inversion with small spikes. (a) Echogram and (b) its FFT.

Fig. 4.   Inversion with tall spikes. (a) Echogram and (b) its FFT.
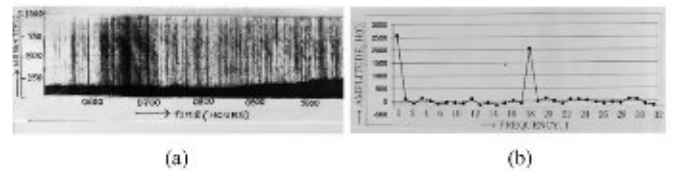

Fig. 5.   Rising inversion. (a) Echogram and (b) its FFT.
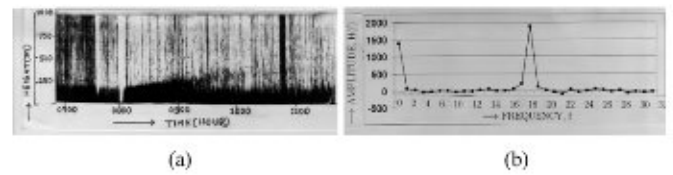

Fig. 6.   Rising inversion with convective plumes. (a) Echogram and (b) its FFT.

with a flat top. This type of layer is generated on clear nights (associated with very light wind condition) due to the emission of infrared radiations from the ground, and is observed during all the four seasons whenever the mechanical turbulence due to wind is negligible.

Fig. 3(a) shows the formation of a temperature inversion layer with small spikes, due to small-scale mechanical turbulence caused by wind of moderate speed. Sometimes, under very high wind conditions, the temperature inversion layer may be associated with tall spikes as observed in Fig. 4(a). The strong mechanical turbulence leads to instability in the atmospheric structure.

Rising inversion of Fig. 5(a) occurs throughout the year during cloudless, clear sunny days, and is associated with a drastic change in the thermodynamic state and pollution density of the LPBL. Fig. 6(a) depicts the rising inversion layer capping a convective boundary layer. The formation of thermal plumes signify that transition of lower atmosphere from stable to unstable state has been completed, and the transfer of heat, momentum, and energy now takes place freely between the earth's surface and the higher levels.

III. IMPLEMENTATION AND RESULTS

In this SODAR system, a pulsed signal (obtained by a tone-burst generator) is amplified in a commercial audio amplifier (135 W) and transmitted vertically upward through

an acoustic transducer placed at the focus of a 6-ft diameter parabolic fiberglass dish antenna. The backscattered signals are recorded by the same antenna, and amplified by a remote preamplifier. Amplified signal, after proper filtration of noise, is fed to the receiver. Finally, a facsimile recorder is used to record the backscattered energy on electrosensitive chart paper as a function of height and time (h, t). The width of the paper describes the height scale (the vertical length of the atmosphere probed by the SODAR, i.e., 1 km, for the system described here), whereas the length of the paper denotes the time scale. The numerical value of the average height of the backscattered sound energy at a particular instant can be obtained from the chart paper in height-time (h, t) domain.

We selected 3-h duration of data from each of the six categories, as depicted in Figs. 1–6. These correspond to the six output classes. The observation was digitized to get the numerical value of average height of backscattered sound energy at intervals of 2 min. In this manner, 90 data points were obtained from the chart of each category. The input data, here, corresponds to overlapping sets of 64 consecutive measurements (height returns of SODAR signal) from each SODAR class. For example, from the sequence of values provided for one SODAR class, the set 1 to 64 form one pattern, 2 to 65 the second pattern, and so on. Next, one-dimensional FFT is applied to transform the SODAR data to its frequency domain, using (2), and these 64 components are used as the input features. A random training set is selected from among this set of input patterns (64 consecutive values) for each class.

A three-layered MLP, with standard backpropagation learning, was used for classifying the patterns. Sixty-four nodes were employed at the input. Investigation was also made with 16 and 32 sequential observations from the frequency domain, but the results were not satisfactory. Six nodes were involved at the output layer, corresponding to the six output classes.

Various three-layered networks were used with different numbers of hidden nodes (20, 25, 30, 35, 40) and training sets (20%, 30%, 40%, 50%). Results are provided in Table I, in terms of recognition score (percent), for the training as well as testing sets. The training set size $x\%$ refers to random, classwise selection of $x\%$ training data from the entire dataset. The remaining $(100 - x)\%$ data constitute the test set in each case.

However, results obtained here may be somewhat biased, as any two input pattern vectors are often overlapping by around 38 data points. This could be avoided by choosing the input pattern vectors of a particular class from different SODAR echograms belonging to that class. But this requires collection of SODAR echograms on a larger scale. On the other hand, the preservation of SODAR echograms is fairly expensive, as each and every echogram must be photographed to save its fading due to seasonal changes. In the current work, we have extended a preliminary study [1] by using FFT to improve the generalization of connectionist classification for SODAR patterns. In the next phase, we plan to extend the work by collecting more number of SODAR echograms, belonging to different classes, for the purpose of investigation.

Table II provides a comparative study on the recognition score (percent) of an MLP, with and without the use of the FFT-based features. Results demonstrate that features representing input pattern vectors directly from the time domain (h, t) provide poor generalization, as compared to incorporation of FFT based inputs. The recognition score for the model in [1] varies between 66.11% and 75.52% over the test set. The FFT-based model, on the other hand, has classification performance over test set ranging from 70.39% to 91.32%. This leads us to infer that the use of FFT at the input, provides overall improved performance as compared to [1].

TABLE I
RECOGNITION SCORES (PERCENT) FOR SODAR DATA, USING FFT-BASED MLP

Train set %	# Nodes Class	20		25		30		35		40	
		Train	Test	Train	Test	Train	Test	Train	Test	Train	Test
20%	1	87.21	70.89	97.40	71.05	95.43	83.71	97.98	44.20	88.33	57.9
	2	89.06	24.80	92.2	58.90	24.24	96.71	94.41	71.49	89.91	42.46
	3	88.33	49.77	99.48	98.37	44.56	78.62	98.65	84.98	89.92	99.90
	4	89.13	9.83	96.38	90.60	94.56	77.63	98.78	77.40	89.96	98.95
	5	85.99	99.32	99.34	72.10	88.42	52.03	98.32	48.39	95.03	81.30
	6	84.96	44.67	98.41	44.77	87.42	78.90	94.93	70.88	89.19	45.37
	Total	90.03	51.20	99.92	82.60	92.48	91.33	98.60	73.02	97.25	72.67
30%	1	98.65	77.10	99.06	91.90	98.46	96.10	95.42	13.40	91.63	82.00
	2	98.98	99.32	93.39	84.60	93.26	91.80	93.69	90.0	89.78	99.44
	3	98.90	99.35	98.24	80.60	99.09	86.80	96.67	90.60	89.99	99.75
	4	98.23	83.62	96.2	88.60	99.06	80.60	96.32	66.42	89.92	78.76
	5	88.86	84.95	94.92	78.38	99.63	78.70	98.1	93.83	85.28	83.9
	6	87.33	90.71	97.9	78.39	26.24	91.18	94.19	78.23	88.32	82.46
	Total	88.26	82.01	92.88	78.40	94.41	88.83	98.73	81.46	88.55	82.48
40%	1	96.33	74.36	99.53	98.35	98.82	95.19	98.29	91.94	97.03	78.45
	2	98.98	97.00	99.90	98.79	93.86	99.54	95.96	99.84	98.22	99.27
	3	99.23	97.44	99.90	80.36	99.40	97.87	95.47	99.00	99.69	99.70
	4	99.68	93.87	99.90	81.77	90.26	99.67	98.16	60.92	98.13	92.62
	5	98.65	77.48	98.30	64.24	98.26	98.80	94.21	58.37	98.25	98.32
	6	97.99	97.11	97.23	87.17	84.23	42.83	95.80	72.90	96.25	44.00
	Total	97.76	98.28	99.60	88.82	98.76	90.31	97.14	91.52	98.45	88.70
50%	1	98.03	88.76	97.48	98.37	99.42	83.39	97.98	99.44	94.75	88.72
	2	99.39	97.02	99.38	99.65	92.82	99.73	97.09	99.34	90.93	99.30
	3	99.09	98.46	99.92	98.51	92.96	99.63	98.36	99.72	97.29	99.72
	4	97.68	97.01	99.87	98.76	97.82	86.58	97.41	93.82	99.21	93.03
	5	98.65	99.42	98.45	98.60	98.84	83.93	98.21	68.22	94.01	86.90
	6	99.99	59.48	97.24	96.79	98.82	78.68	99.14	60.95	97.32	50.48
	Total	99.24	84.01	98.90	91.32	99.06	91.97	97.96	85.21	97.39	85.80

TABLE II
RECOGNITION SCORES (PERCENT) FOR SODAR DATA

Training set	Hidden nodes	MLP [1]		FFT–MLP	
		Train	Test	Train	Test
20%	20	98.23	71.47	96.21	81.28
	25	98.98	69.71	93.99	82.00
	30	98.50	68.11	99.23	81.32
	35	98.23	68.53	99.60	70.39
30%	20	99.49	69.63	98.95	87.06
	25	100.00	68.63	99.66	79.40
	30	99.11	69.23	99.11	85.04
	35	97.35	68.92	98.73	81.46
40%	20	97.95	71.07	97.51	86.28
	25	97.44	71.28	99.49	85.02
	30	97.90	72.69	98.75	90.01
	35	98.25	71.07	97.4	91.32
50%	20	97.44	71.28	99.23	86.01
	25	98.70	72.69	98.96	91.31
	40	99.52	75.52	99.66	90.07
	75	98.42	66.83	99.06	84.21

IV. Conclusion and Discussion

The sound radar or SODAR system has emerged as a useful and cost-effective tool that provides information about the formation of different types of temperature inversion layers, thermal plumes, fog layer, elevated temperature inversion layers, and various other types of lower atmospheric structures, on a continuous basis. However, the identification of SODAR echograms is time-consuming and can be performed only by the experts having wide experience in this domain. Hence the need for automated systems was evident, leading to the design of an MLP for the purpose.

In this initial step, we observed that it was difficult to get good classification and generalization with the raw dataset available in the height-time (h, t) domain [1]. In order to improve the results, a sample of 64 consecutive data points from each class was subjected to FFT for obtaining the inputs from the frequency domain. The improved results of Table II validate this claim.

It is conjectured that the design of such an automated system may enable us to make potential use of SODAR data. At the same time, this holds promise for researchers working in the areas of atmospheric sciences, meteorology, air pollution meteorology, civil aviation, microwave propagation, remote sensing, and various other related fields.

Acknowledgment

References

[1] S. Choudhury and S. Mitra, "A connectionist approach to SODAR pattern classification," *IEEE Geosci. Remote Sens. Lett.*, vol. 1, no. 1, pp. 42–46, Jan. 2004.

[2] L. G. Mcallister, J. R. Pollard, A. R. Mahohey, and P. J. R. Shaw, "A new approach to the study of atmospheric structure," *Proc. IEEE*, vol. 57, no. 4, pp. 579–587, Apr. 1969.

[3] C. G. Little, "Acoustic methods for the remote probing of the lower atmosphere," *Proc. IEEE*, vol. 57, no. 4, pp. 571–578, Apr. 1969.

[4] S. Haykin, *Neural Networks: A Comprehensive Foundation*. New York: Macmillan, 1994.

[5] J. T. Tou and R. C. Gonzalez, *Pattern Recognition Principles*. Reading, MA: Addison-Wesley, 1974.

[6] C. Marzban and G. J. Stumpf, "A neural network for tornado prediction based on Doppler radar-derived attributes," *J. Appl. Meteorol.*, vol. 35, pp. 617–626, 1996.

[7] ——, "A neural network for damaging wind prediction," *Weather Forecast.*, vol. 13, pp. 151–163, 1998.

[8] S. Choudhury, S. Mitra, and S. K. Pal, "Neuro-fuzzy classification and rule generation of modes of radiowave propagation," *IEEE Trans. Antennas Propagat.*, vol. 51, no. 4, pp. 862–871, Apr. 2003.

[9] A. Pal, S. Choudhury, N. C. Deb, and M. Dey, "Some Pattern Recognition Issues in Acoustic Sounding," Indian Stat. Inst., Appl. Stat. Div., Kolkata, Tech. Rep. ASD/2002/1, 2002.

[10] A. Mukherjee, P. Pal, and J. Das, "Classification of SODAR data using fractal features," in *Proc. 3rd Indian Conf. Computer Vision, Graphics and Image Processing*, 2002, pp. 203–207.

[11] W. H. Press, S. A. Teukolsky, W. T. Vetterling, and B. P. Flannery, *Numerical Recipes in C: The Art of Scientific Computing*. Cambridge, U.K.: Cambridge Univ. Press, 1995.

[12] J. W. Cooley and J. W. Tukey, "An algorithm for the machine calculation of complex Fourier series," *Math. Comput.*, vol. 19, pp. 297–301, 1965.